Journal of Molecular Liquids 313 (2020) 113509

Contents lists available at ScienceDirect

Journal of Molecular Liquids

journal homepage: www.elsevier.com/locate/molliq

Experimental and DFT/TD-DFT computational investigations of the solvent effect on the spectral properties of nitro substituted pyridino [3,4-*c*]coumarins

Mohanad Shkoor, Hanin Mehanna, Ayaa Shabana, Toka Farhat, Abdulilah Dawoud Bani-Yaseen *

Department of Chemistry & Earth Sciences, Faculty of Arts & Science, Qatar University, P.O. Box: 2713, Doha, Qatar

ARTICLE INFO

Article history:
Received 8 May 2020
Received in revised form 23 May 2020
Accepted 2 June 2020
Available online 5 June 2020

Keywords:
Pyridino[3,4-*c*]coumarins
Absorption spectroscopy
Solvatochromism
Molecular modeling
DFT and TD-DFT

ABSTRACT

The UV/Vis absorption characteristics of newly synthesized pyridino[3,4-c] coumarins in different neat solvents were investigated experimentally and computationally. It is noted that the nitro-substituted pyridocoumarins can exhibit spectral features with characteristic band in the visible region, which in turn is solvent's polarity dependent with negative solvatochromic behavior. Using the Kamet-Taft approach, the obtained results ($R = 0.991$) revealed that this negative solvatochromic behavior is dominantly influenced by the solvents' polarizability and hydrogen bonding capability. The experimental results of the spectral properties in solution were interpreted at the molecular level with aid of the DFT and TD-DFT/CAM-B3LYP/6-31+G(d) computational methods with IEFPCM implicit solvation approach. Per benchmarking the TD-DFT simulated spectra with the experimental one, it is demonstrated that the nitro group can induce an intramolecular charge transfer to afford two resonance structures of distinctive spectral features. Such difference in spectral features is interpreted in terms of molecular orbitals, where the two potential resonance structures exhibit different natures for the frontier molecular orbitals, namely the HOMO and LUMO with a significant difference in the corresponding energy gaps. Moreover, the electrostatic potential surfaces of both structures indicate relatively different accessibility toward intermolecular hydrogen bonding with the solvent molecules. The achieved results would provide valuable insights concerning the noteworthy influence of the substituents of pyridocoumarins on their spectral properties and correspondingly their solvatochromic behaviors at the molecular level in different media.

1. Introduction

Coumarin (2*H*-cromen-2-one) is a pivotal heterocyclic framework that is widely present in bioactive natural products [1–3]. In addition, coumarin is found in bioactive molecules that exhibit various pharmaceutical activities, such as antioxidant [4], anti-inflammatory [5], antibacterial [6], antiviral [7], antitumor [8], and other activities [9–12]. In fact, many coumarin-based compounds are commercial drugs for example, the traditional anticoagulant drug warfarin. In addition to the wide spectrum of biological activities, coumarin is present in the structures of many insecticides [13], and food additives [14]. Because substituted coumarins display high florescent quantum yield and respond to their microenvironments [15,16], coumarin-containing compounds exhibit a variety of important photophysical properties that render coumarins valuable molecules as fluorescent sensors [17], optical devices [18–20], fluorescence dyes [21,22] and laser dyes [23,24].

Amongst fused coumarins, pyridino[3,4-*c*]coumarins are considered as an important class of pyridocoumarins family [25] that are found in several natural products and bioactive molecules [25]. Moreover, pyridino[3,4-*c*]coumarins display various pharmaceutical activities including, antiviral [26], antimicrobial and anti-inflammatory [27], Antipsychotic [28] and antibacterial [29] properties. For a better understanding of the behavior of these interesting molecules, On the other hand, spectral investigations of such important compounds can provide valuable information concerning their physicochemical properties [30–32]. Such information in turn is significant toward interpreting and understanding the change in electronic distribution and geometrical structure upon excitation, charge distribution, electrophilic and nucleophilic sites in potential chemical reactions, and solvent polarity [33,34]. Thus, solvatochromism is the most utilized technique to determine such properties of molecules at the ground state and after excitation [35]. This exciting phenomenon involves measuring the electronic spectra of the probes in various solvents with variable polarities and hydrogen bond donor/acceptor capabilities [30,33,35], where the solvent-probe interaction is observed mainly as a change in the shape and intensity of the electronic spectral bands [36–38].

In the study reported herein, we attempted to investigate the physicochemical properties of two newly synthesized pyridocoumarins via examining the solvent effects on their UV–Vis absorption spectra

* Corresponding author.
E-mail address: abdulilah.baniyaseen@qu.edu.qa (A.D. Bani-Yaseen).

https://doi.org/10.1016/j.molliq.2020.113509

experimentally and computationally. The chemical structures of these compounds are shown in Fig. 1. The absorption spectra were measured eight neat solvents, where the solvent's polarizability and hydrogen bonding (HB) capabilities were assessed employing the Kamlet-Taft and multilinear regression analysis (MLRA). The DFT and TD-DFT computational methods were employed to provide insights concerning the physicochemical properties of these compounds at the molecular level. In the light of the computational study and per the good agreement with the experimental results, the resonance structures and the type of spectral bands in solution for the nitro substituted pyridocoumarins were highlighted and discussed.

2. Experimental

2.1. Materials

Solvents were supplied by Sigma-Aldrich, and used without further purification. All organic solvents, namely ethanol, methanol, isopropanol, ethylacetate, acetonitrile, 1,4-dioxane, and acetone were of spectroscopic grades.

2.2. Synthesis

Syntheses of the two derivatives of the substituted pyridino[3,4-*c*] coumarins have been reported previously [39]. The chemical structures are shown in Fig. 1.

2.3. Procedures and spectroscopic measurement

Stock solutions (3.0×10^{-4} M) in methanol were prepared for each compound. The working solution of approximately 3.0×10^{-6} M was prepared by withdrawing an aliquot of the stock solution prepared in methanol, then setting the system for evaporation under ambient pressure at room temperature. The residue then was re-dissolved in appropriate volume of the solvent of interest. The UV–Vis absorption spectra of the synthesized compounds were measured in neat organic solvents and ultrapure deionized water using Agilent double beam spectrophotometer in quartz cells.

2.4. Computational methods

All DFT and TD-DFT calculations were performed with *Gaussian 09* version D.01. Full Molecular geometry optimization was performed employing the hybrid B3LYP functional and 6-31+G(d) basis set [40]. The implicit solvent effect was considered employing the integral equation formalism polarizable continuum model (IEFPCM) [41]. Simulated absorption spectra were calculated using the time-dependent version of DFT, namely TD-DFT, with CAM-B3LYP functional and 6–31 + G (d) basis set. The simulated absorption spectra were calculated for the first eighteen excitation states using the optimized ground-state geometry as an input geometry. The multilinear regression analysis (*MLRA*) was performed as implemented in Microsoft Excel.

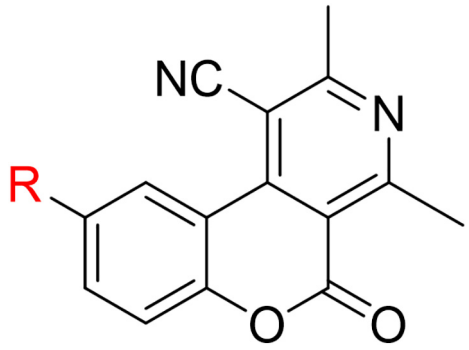

Fig. 1. Chemical structure of pyridino[3,4-*c*]coumarins, **I**, R = H; **II**, R = NO_2.

3. Results and discussion

3.1. UV–Vis absorption spectra

The absorption spectra for the two tested compounds I and II in water and acetonitrile (structures are displayed in Fig. 1) are shown in Fig. 2. Spectra were measured in water and acetonitrile as an initial assessment for the effect of solvent polarities on the spectral properties of I and II. The absorption spectrum of I in acetonitrile exhibits features of three bands; two main bands at a wavelength (λ) of 247 and 317 nm, and one shoulder at approximately 275 nm. In terms of the position of the band, the absorption spectrum of I in water contains similar features but with a shoulder shape for all bands. Hence, although the absorption spectra of I exhibited solvent dependency in terms of the shape of the bands, no solvatochromic behavior was observed for I concerning the position of the corresponding bands.

On the other hand, one can notice that both spectra of I and II can exhibit some similarities within the range of 200–340 nm. However, a significant characteristic difference can be noted for II with the appearance of a new band within the visible range of 400–430 nm. Importantly, per the structure of I and II, it is evident that the incorporation of nitro group is responsible for the appearance of this band. Furthermore, as this band is the main band that is notably affected by the solvent within the visible range, this band will be referred to as $\lambda_{max,v}$. Interestingly the position of this band is solvent polarity dependent, where a $\lambda_{max,v}$ of 401 and 418 nm were observed in water and acetonitrile, respectively. As such, the solvatochromic behavior of II was further investigated in solvents of different polarities.

3.2. Solvatochromic behavior of compound II

The effect of solvents on the absorption spectra of II was studied in eight neat solvents of various polarities and hydrogen bonding capabilities and within the range between 200 and 500 nm; these solvents include water, methanol ethanol, isopropanol, acetonitrile, ethyl acetate,

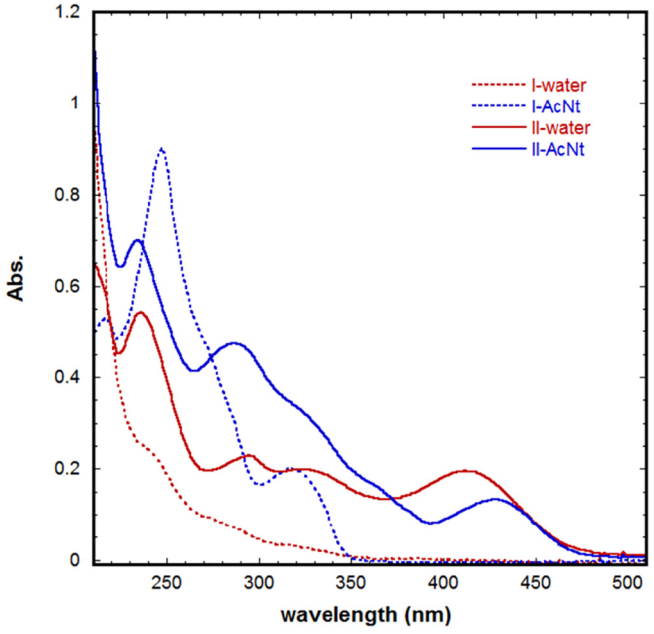

Fig. 2. Absorption spectra of compounds I and II in water and acetonitrile.

acetone, and 1,4-dioxane. The selected solvents typically are categorized into three groups, as listed in Table 1, namely polar protic, polar aprotic, and nonpolar. Fig. 3 shows the measured absorption spectra in the selected solvents and were normalized to unity with respect to $\lambda_{max,v}$.

As shown in Fig. 3, it can be noted that a significant hypsochromic shift of approximately 10–40 nm was observed for $\lambda_{max,v}$ as solvent polarity increases amongst the tested solvents indicative of negative solvatochromic behavior. Also, this band disappears in two solvents namely 1,4-dioxane and ethylacetate. Typically, this spectral shift in $\lambda_{max,v}$ occurs because of the intermolecular interactions between the molecule and solvent; this includes dipole-dipole interactions and hydrogen bonding (HB).

In order to demonstrate the influence of both factors on the spectral shift of $\lambda_{max,v}$, we performed the Kamlet-Taft multilinear regression analysis (MLRA) [42]; the general expression is given in Eq. (1).

$$\lambda_{max} = \lambda_o + a\alpha + b\beta + c\pi^* \quad (1)$$

where λ_{max} is the absorption maximum under solvent effect, λ_o is regression intercept that agrees with gaseous phase, α reflects the hydrogen bond donor acidity (HB_D), β is the hydrogen bond acceptor basicity (HB_A) and π^* is an index of solvents dipolarity/polarizability which is the ability of solvents to stabilize the dissolved dipole or charge [24]; a, b and c are independent constants and their signs and magnitudes help in determining the effect of the corresponding solvent-solute interactions on the maximum absorption wavelength. The MLRA for $\lambda_{max,v}$ was performed and expressed in Eq. (2).

$$\lambda_{max,v} = 371(\pm 18) - 33(\pm 4)\alpha + 47(\pm 13)\beta + 54(\pm 18)\pi^* \quad R = 0.990 \ (2)$$

It is worth to mention that the MLRA was performed for the solvents in which clear $\lambda_{max,v}$ is observed as listed in Table 1. As such, two solvents were not included in the MLRA namely ethylacetate and 1,4-dioxane. Interestingly, the results obtained from the MLRA as expressed in Eq. (2) are indicative of major contributions of not only the polarity of the solvent, but also the HB effects with negative and positive coefficients for HB_A and HB_B, respectively. Comparing the values for α and β for all tested solvent, it is obvious that α is more dominant for protic solvents. With a negative coefficient of 33 for α, it is evident that HB_A has a significant contribution in inducing a hypsochromic shift in $\lambda_{max,v}$ for compound II. Based on these findings, it can be suggested that the dipole-dipole interactions and HB can lead to ionic coupling and solvation within the molecular environment of compound II, and consequently these two factors influencing the solvatochromic behavior of $\lambda_{max,v}$. In addition, with the excellent correlation coefficient (R) of 0.992 obtained for the MLRA as indicated by Eq. (2), the acquired module was employed for predicting $\lambda_{max,v}$ in the same tested solvents. Fig. 4 displays the correlation between the measured and predicted $\lambda_{max,v}$. It is interesting to notice that an excellent correlation was obtained with $R = 0.991$ indicative of the validity of the employed approach. However, such observation for compound II still necessitates further analysis using selected methods of computational chemistry toward rationalization of the solvent effect on its spectral properties.

Table 1
Solvent parameters and spectral properties of **II**.

Solvent	α	β	π*	λ_{max1}, nm	$\lambda_{max,v}$ (nm)
Polar protic					
Water	1.17	0.18	1.09	286	400
Methanol	0.93	0.62	0.60	287	404
Ethanol	0.83	0.77	0.54	285	408
Isopropanol	0.76	0.95	0.48	286	416
Polar aprotic					
Acetone	0.08	0.48	0.71		431
Ethylacetate	0	0.45	0.55	276	
Acetonitrile	0.19	0.31	0.75	277	418
Nonpolar					
1,4-Dioxane	0	0.37	0.55	283	

3.3. DFT/TD-DFT and molecular orbitals characteristics

The negative solvatochromic behavior is indicative of the fact that the dipole moment of the molecule in the ground state (μ_g) is higher than in the excited state. Hence, the increase in the solvent polarity causes further stabilization in the ground state energy and in turn increases the energy gap between the ground and excited states and consequently a shorter wavelength is observed for the absorption spectrum

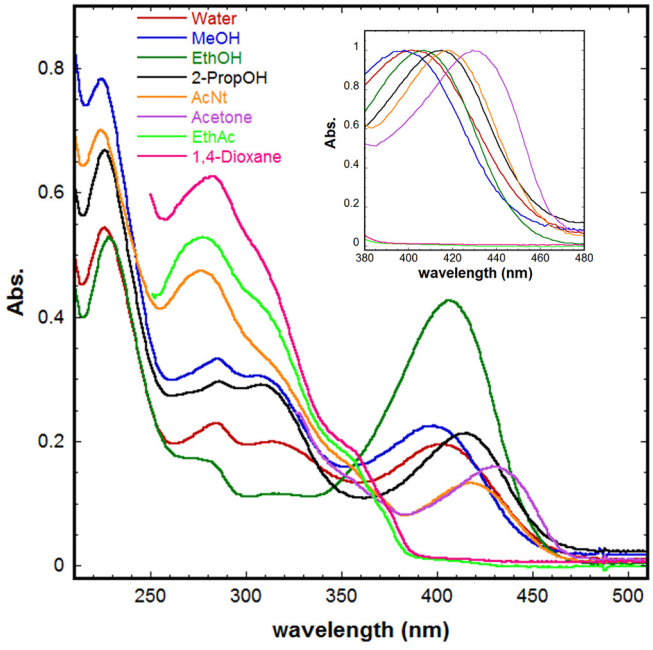

Fig. 3. Absorption spectra of compounds II in neat solvents; inset: normalized spectra with respect to the band in the visible range.

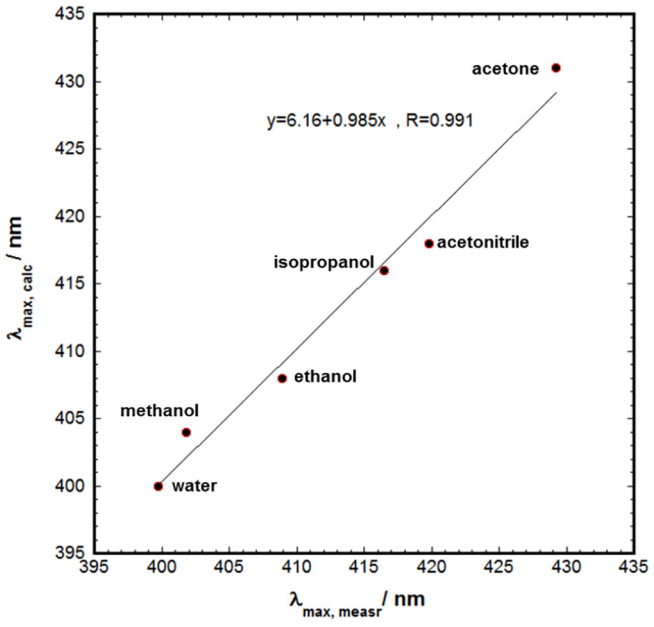

Fig. 4. Correlation between predicted and measured $\lambda_{max,v}$ for compound II in neat solvents.

of the molecule of interest such as compound II in this study. On the other hand, as mentioned above, compound II is different from I by the incorporation of the nitro group, which in turn has significantly changed the spectral features of the compound by the appearance new band in the visible range. To this end, DFT and TD-DFT calculations were conducted to gain insights concerning the key molecular orbital (MO) that are associated with the absorption spectra and the corresponding electronic states and transitions of compound II. We emphasize herein on the role of the nitro group and solvent effects in particular.

It is noteworthy mentioning that such negative solvatochromic behavior for $\lambda_{max,v}$ may often be indicative for $n \rightarrow \pi^*$ electronic transition. However, the observed variations in the spectral properties of II by the incorporation of the nitro group can also be attributed to the fact that the nitro group is included in possible resonance structures of II. Optimized geometries for proposed resonance structures of II are displayed in Fig. 5. The main difference amongst these resonance structures is the involvement of the nitro group, where for II-A and II-B correspond to the nitro group to be nonconjugated and conjugated with the benzene ring, respectively. The given numbers in those geometries refer to the NBO atomic charges for the atoms that are most likely involved in the corresponding resonance structures. Such resonance structures may in fact be produced by an intramolecular charge transfer (ICT) that causes a further stabilization in the energy of the ground state of the corresponding absorption band and consequently a decrease in $\lambda_{max,v}$. Furthermore, one can notice approximately a 24–31% reduction in the NBO values of two carbon atoms of the nitro-substituted benzene ring for II-B indicative of charge redistribution over the resonance structures induced by the nitro group.

This kind of charge redistribution over II induced by the nitro group was further examined through performing a TD-DFT study for the two possible resonance structures, namely II-A and II-B. Fig. 6 shows the experimental and simulated absorption spectra of II-A and II-B. Per benchmarking the simulated spectra against the experimental one, the existence of such kind of resonance structures is demonstrated. The vertical dotted lines correspond to the electronic transition between MOs responsible for the absorption band with oscillation frequency (f) which is ≥0.1, where the height of the line represents the relative value for f. It can be noted that the simulated band of II-B at 347 nm

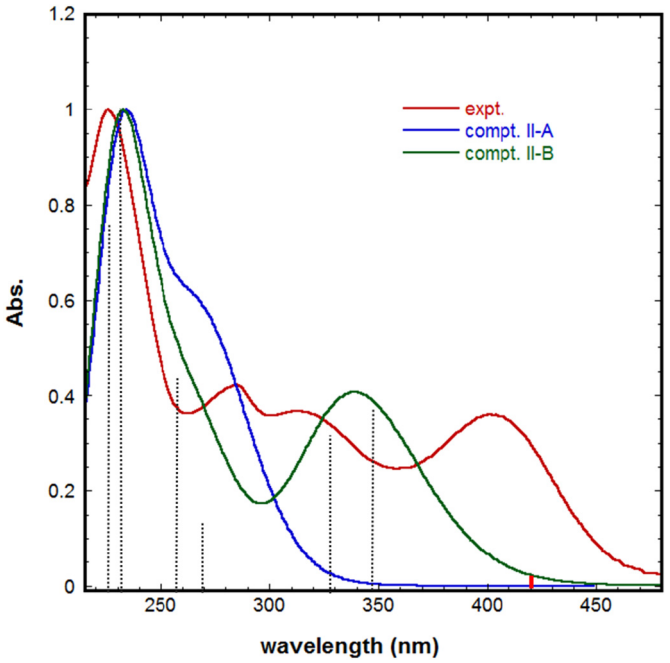

Fig. 6. Experimental and TD-DFT (DFT (CAM-B3LYP/6-31G+(d), IEFPCM)) simulated absorption spectra of the two resonance structures of II (II-A, II-B) in water.

resembles the band of $\lambda_{max,v}$, which in turn is produced dominantly HOMO→LUMO transition with less contribution of HOMO-2 → LUMO transition. However, other kinds of transitions must be considered as well.

Importantly, it must be mentioned that the TD-DFT calculations revealed a transition at a wavelength of 429 nm of low f, which highlighted in Fig. 6 with a red vertical line. Although a small value of f is calculated for simulated transition at a wavelength of 429 nm, it is suggested that this transition corresponds to $n \rightarrow \pi^*$ transition, which in turn necessitates further demonstration via MOs analyses. Moreover, to account for the role of the nitro group in terms of MOs, the frontier orbitals HOMO and LUMO were generated as well as other MO that

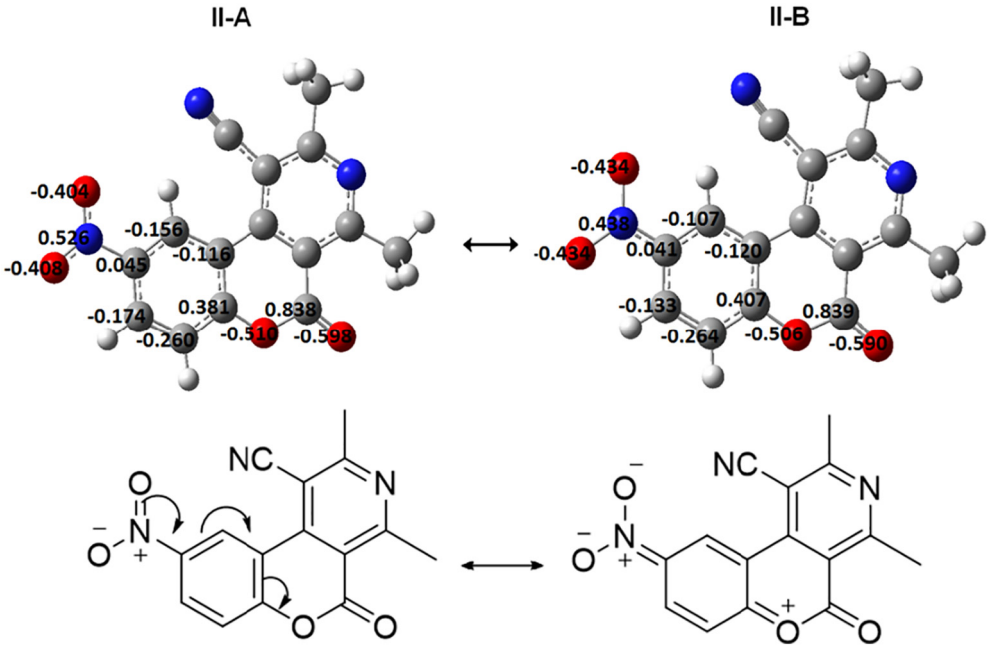

Fig. 5. Suggested resonance structures and the corresponding DFT (B3LYP/6-31G+(d), IEFPCM) optimized geometries in water, numbers indicate the NBO atomic charges of selected atoms.

are associated with the spectral features of compound II using the DFT method.

Fig. 7 displays selected MOs of both resonance structures including HOMO and LUMO. Interestingly, it can be concluded that both structures exhibit HOMO → LUMO transitions that are of the type π → π* transitions, which appear within the UV range of the spectrum. However, the longer wavelength obtained for II-B is notably in better agreement with the experimental results. It must be noted that the significant difference in the features of the simulated spectra of both structures can be attributed to the fact that the LUMO, where most of the electronic transition are directed to, is of different nature. For II-A, the LUMO is the π* MO of a regular C═C bond within an aromatic ring, whereas for II-B it is the π* MO of C═O that is yielded because of the resonance process involving the nitro group. With the correspondence of the HOMO(−4) → LUMO, it can be concluded that the conjugation of the nitro group with the aromatic moiety of compound II-B may enhance the probability of new electronic transitions and consequently the appearance of the new absorption band of $\lambda_{max,v}$.

Furthermore, we attempted to rationalize the effect of solvent polarity on the position of $\lambda_{max,v}$ through comparing the simulated absorption spectra of II-B in water with those obtained in vacuum and acetonitrile. Interestingly, no difference was noted for the shape of HOMO and LUMO. However, a minor difference was observed for the energy of the HOMO(−4) → LUMO transitions, where ΔE decreased by 0.008 eV in acetonitrile compared with water. Such an increase in ΔE as observed in water compared with acetonitrile indicative of a hypsochromic shift in $\lambda_{max,v}$, which in turn is in good agreement with the experimental results, where a hypsochromic shift is observed with increasing solvent polarity. In addition, the obtained results revealed that such an increase in ΔE in water compared with acetonitrile is attributed to more stabilization of the HOMO(−4), which is in good agreement with the experimental findings where a negative solvatochromism is often attributed to stabilization of the ground state.

The polarization of the resonance structures of II was further assessed through the electrostatic potential surface (EPS) using the DFT method. Generally, the EPS presents the degree of charge separation across the molecule, where the red and blue colors regions indicate negative and positive, respectively, and electrostatic potentials. Importantly, the aforementioned color codes do not only indicate the regions of the molecule for potential electrophilic and nucleophilic reactions, but also the accessibility for intermolecular interactions including HB. Fig. 8 shows the EPS of both resonance structures of compound II.

The EPSs of both resonance structures show that the electron density in both structures is accumulated in the same regions including the nitro group as indicated by regions with the red color. This in turn indicates that both structures have similar accessible regions for intermolecular HB with the solvent molecules. However, the more charge separation obtained for II-B is consistent with an increase of in μ_g, where values of 5.1 and 7.2 Debye were obtained for II-A and II-B respectively. With this increase in charge separation and μ_g for II-B, it can be suggested that the nitro group has relatively become more accessible for the solvent molecules for intermolecular interaction via HB. As such, stabilization of the ground state occurs and consequently the n → π* is shifted toward shorter wavelength, which in turn is in good agreement with e the experimental results.

4. Concluding remarks

The present work investigated the influence of solvents on the UV–Vis absorption spectral properties of two newly synthesized pyridocoumarins of different substituents. Characteristic spectral features were observed for the nitro-substituted pyridocoumarin compared with the other H- pyridocoumarin, where a new band appeared in the visible range that is defined as $\lambda_{max,v}$. This new band exhibited notable negative solvatochromic behavior, where $\lambda_{max,v}$ decreases with increasing solvent polarity. However, the MLRA analyses performed using the Kamlet-Taft approach have demonstrated that the solvent polarizability is not the only key factor triggering negative solvatochromic behavior, but also HB capabilities of the solvent. The experimental spectra in solution were reproduced employing TD-DFT/CAM-B3LYP/6-31+G(d) computational methods with IEFPCM implicit solvation approach. It is demonstrated that the new band is attributed to resonance structures induced by ICT with significant contribution from the nitro group, where the nitro group is conjugated with the benzene ring of the coumarin moiety. Interestingly, the nitro group has significantly changed the orientations of the MOs including the frontier MOs, namely HOMO and LUMO, with a notable change in energy gap compared with the other resonance structure. As such, different spectral features were observed for the nitro-

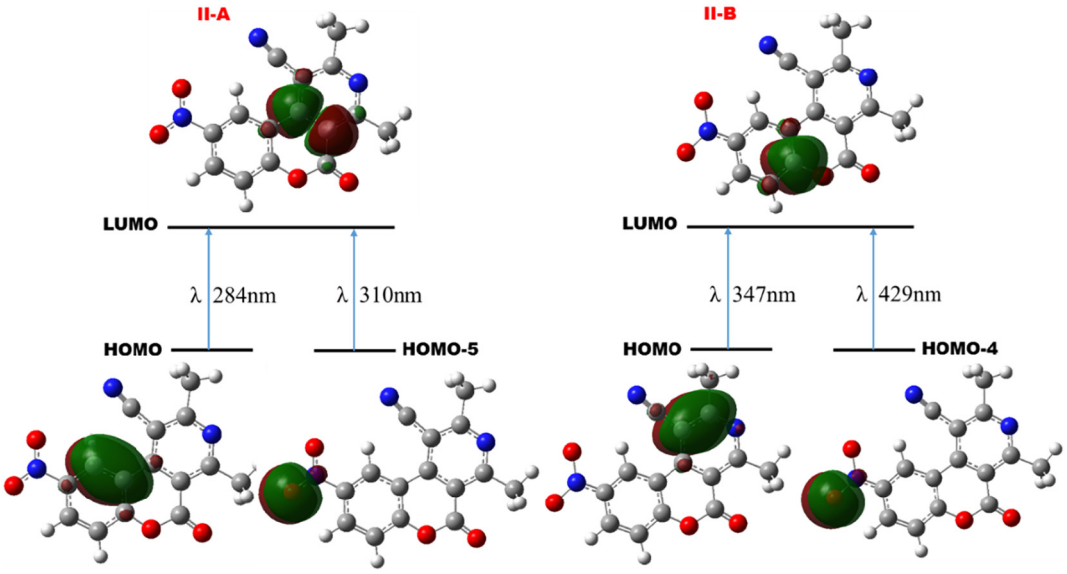

Fig. 7. Selected MOs of II-A and II-B and the corresponding electronic transitions; DFT (B3LYP/6-31G+(d), IEFPCM).

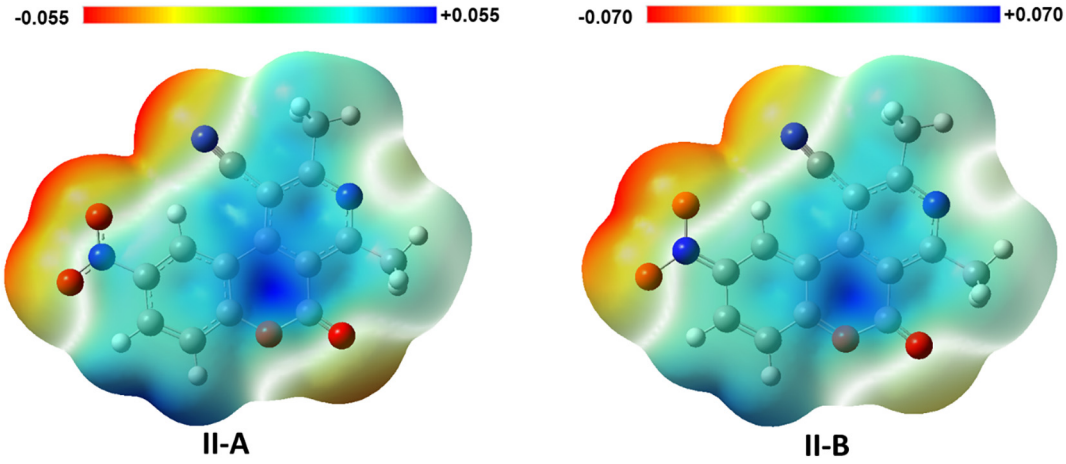

Fig. 8. Electrostatic Potentials Surfaces (EPS) of resonance structures II-A and II-B; DFT (B3LYP/6-31G+(d), IEFPCM).

substituted pyridocoumarins with a solvent's dependency spectral characteristics.

Declaration of competing interest

The authors report no relationships that could be construed as a conflict of interest.

Acknowledgements

The support from Qatar University is thankfully acknowledged.

References

[1] B. Fois, S. Distinto, R. Meleddu, S. Deplano, E. Maccioni, C. Floris, A. Rosa, M. Nieddu, P. Caboni, C. Sissi, A. Angeli, C.T. Supuran, F. Cottiglia, Coumarins from Magydaris pastinacea as inhibitors of the tumour-associated carbonic anhydrases IX and XII: isolation, biological studies and in silico evaluation, J. Enzyme Inhib. Med. Chem. 35 (2020) 539–548, https://doi.org/10.1080/14756366.2020.1713114.

[2] J.-J. Zhu, J.-G. Jiang, Pharmacological and nutritional effects of natural coumarins and their structure-activity relationships, Mol. Nutr. Food Res. 62 (2018), 1701073. https://doi.org/10.1002/mnfr.201701073.

[3] R.A. Davis, D. Vullo, A. Maresca, C.T. Supuran, S.-A. Poulsen, Natural product coumarins that inhibit human carbonic anhydrases, Bioorg. Med. Chem. 21 (2013) 1539–1543, https://doi.org/10.1016/j.bmc.2012.07.021.

[4] B.Z. Kurt, I. Gazioglu, N.O. Kandas, F. Sonmez, Synthesis, anticholinesterase, antioxidant, and anti-aflatoxigenic activity of novel coumarin carbamate derivatives, ChemistrySelect 3 (2018) 3978–3983, https://doi.org/10.1002/slct.201800142.

[5] H. Fan, Z. Gao, K. Ji, X. Li, J. Wu, Y. Liu, X. Wang, H. Liang, Y. Liu, X. Li, P. Liu, D. Chen, F. Zhao, The in vitro and in vivo anti-inflammatory effect of osthole, the major natural coumarin from Cnidium monnieri (L.) Cuss, via the blocking of the activation of the NF-κB and MAPK/p38 pathways, Phytomedicine 58 (2019), 152864. https://doi.org/10.1016/j.phymed.2019.152864.

[6] K. Bhagat, J. Bhagat, M.K. Gupta, J.V. Singh, H.K. Gulati, A. Singh, K. Kaur, G. Kaur, S. Sharma, A. Rana, H. Singh, S. Sharma, P.M. Singh Bedi, Design, synthesis, antimicrobial evaluation, and molecular modeling studies of novel indolinedione–coumarin molecular hybrids, ACS Omega 4 (2019) 8720–8730, https://doi.org/10.1021/acsomega.8b02481.

[7] S. Mishra, A. Pandey, S. Manvati, Coumarin: an emerging antiviral agent, Heliyon 6 (2020), e03217. https://doi.org/10.1016/j.heliyon.2020.e03217.

[8] A. Bisi, C. Cappadone, A. Rampa, G. Farruggia, A. Sargenti, F. Belluti, R.M.C. Di Martino, E. Malucelli, A. Meluzzi, S. Iotti, S. Gobbi, Coumarin derivatives as potential antitumor agents: growth inhibition, apoptosis induction and multidrug resistance reverting activity, Eur. J. Med. Chem. 127 (2017) 577–585, https://doi.org/10.1016/j.ejmech.2017.01.020.

[9] K.V. Sairam, B.M. Gurupadayya, R.S. Chandan, K.N. Dattatri, B. Vishwanathan, A review on chemical profile of coumarins and their therapeutic role in the treatment of cancer, Curr. Drug Deliv. 13 (2016) 186–201, https://doi.org/10.2174/1567201812666150702102800.

[10] F.G. Medina, J.G. Marrero, M. Macías-Alonso, M.C. González, I. Córdova-Guerrero, A.G. Teissier García, S. Osegueda-Robles, Coumarin heterocyclic derivatives: chemical synthesis and biological activity, Nat. Prod. Rep. 32 (2015) 1472–1507, https://doi.org/10.1039/C4NP00162A.

[11] A. Thakur, R. Singla, V. Jaitak, Coumarins as anticancer agents: a review on synthetic strategies, mechanism of action and SAR studies, Eur. J. Med. Chem. 101 (2015) 476–495, https://doi.org/10.1016/j.ejmech.2015.07.010.

[12] H.M. Revankar, S.N.A. Bukhari, G.B. Kumar, H.-L. Qin, Coumarins scaffolds as COX inhibitors, Bioorg. Chem. 71 (2017) 146–159, https://doi.org/10.1016/j.bioorg.2017.02.001.

[13] S. Chen, M.E.A. Elzaki, C. Ding, Z. Li, J. Wang, R. Zeng, Y.-Y. Song, Plant allelochemicals affect tolerance of polyphagous lepidopteran pest Helicoverpa armigera (Hübner) against insecticides, Pestic. Biochem. Physiol. 154 (2019) 32–38, https://doi.org/10.1016/j.pestbp.2018.12.009.

[14] Y.-H. Wang, B. Avula, N.P.D. Nanayakkara, J. Zhao, I.A. Khan, Cassia cinnamon as a source of coumarin in cinnamon-flavored food and food supplements in the United States, J. Agric. Food Chem. 61 (2013) 4470–4476, https://doi.org/10.1021/jf4005862.

[15] W. Xue, D. Wang, C. Li, Z. Zhai, T. Wang, Y. Liang, Z. Zhang, π-Expanded coumarins: one-pot photo synthesis of 5 H -benzo[12,1]tetrapheno[7,6,5-cde]chromen-5-ones and photophysical properties, J. Org. Chem. 85 (2020) 3689–3698, https://doi.org/10.1021/acs.joc.9b03327.

[16] T. Mikysek, P. Nikolaou, M. Kafexholli, P. Šimůnek, J. Váňa, A. Marková, M. Vala, G. Valenti, Photophysical and electrochemiluminescence of coumarin-based oxazaborines, ChemElectroChem 7 (2020) 1550–1557, https://doi.org/10.1002/celc.201902102.

[17] D. Cao, Z. Liu, P. Verwilst, S. Koo, P. Jangjili, J.S. Kim, W. Lin, Coumarin-based small-molecule fluorescent chemosensors, Chem. Rev. 119 (2019) 10403–10519, https://doi.org/10.1021/acs.chemrev.9b00145.

[18] H.D. Duong, Y. Shin, J. Il Rhee, Development of novel optical pH sensors based on coumarin 6 and nile blue A encapsulated in resin particles and specific support materials, Mater. Sci. Eng. C. 107 (2020), 110323. https://doi.org/10.1016/j.msec.2019.110323.

[19] S. Karmakar, D. Ray, Synthesis, optical properties, acid-base vapochromism and anti-counterfeiting of novel π-extended pyridine fused coumarins, J. Lumin. 223 (2020), 117229. https://doi.org/10.1016/j.jlumin.2020.117229.

[20] E. Bozkurt, Y. Onganer, Optical and morphological characterization of novel coumarin 151 doped polyvinylpyrrolidone thin film, J. Lumin. 205 (2019) 318–323, https://doi.org/10.1016/j.jlumin.2018.09.039.

[21] S. Qi, Q. Li, W. Liu, H. Ren, H. Zhang, J. Wu, J. Ge, P. Wang, Coumarin/fluorescein-fused fluorescent dyes for rapidly monitoring mitochondrial pH changes in living cells, Spectrochim. Acta Part A Mol. Biomol. Spectrosc. 204 (2018) 590–597, https://doi.org/10.1016/j.saa.2018.06.095.

[22] V.V. Annenkov, S.N. Zelinskiy, V.A. Pal'shin, L.I. Larina, E.N. Danilovtseva, Coumarin based fluorescent dye for monitoring of siliceous structures in living organisms, Dyes Pigments 160 (2019) 336–343, https://doi.org/10.1016/j.dyepig.2018.08.020.

[23] V.F. Traven, D.A. Cheptsov, N.P. Solovjova, T.A. Chibisova, I.I. Voronov, S.M. Dolotov, I.V. Ivanov, Photoinduced formation of the laser dye coumarin 6 from its dihydro derivatives, Dyes Pigments 146 (2017) 159–168, https://doi.org/10.1016/j.dyepig.2017.07.001.

[24] D. Stefanska, M. Suski, B. Furmann, Tunable continuous wave single-mode dye laser directly pumped by a diode laser, Laser Phys. Lett. 14 (2017), 045701. https://doi.org/10.1088/1612-202X/aa5f00.

[25] P. Patra, A concise review on pyridocoumarin/azacoumarin derivatives: synthesis and biological activity, ChemistrySelect 4 (2019) 2024–2043, https://doi.org/10.1002/slct.201803596.

[26] P.J. Houghton, T.Z. Woldemariam, A.I. Khan, A. Burke, N. Mahmood, Antiviral activity of natural and semi-synthetic chromone alkaloids, Antivir. Res. 25 (1994) 235–244, https://doi.org/10.1016/0166-3542(94)90006-X.

[27] I.A. Khan, M.V. Kulkarni, M. Gopal, M.S. Shahabuddin, C.-M. Sun, Synthesis and biological evaluation of novel angularly fused polycyclic coumarins, Bioorg. Med. Chem. Lett. 15 (2005) 3584–3587, https://doi.org/10.1016/j.bmcl.2005.05.063.

[28] P.C. Unangst, T. Capiris, D.T. Connor, T.G. Heffner, R.G. MacKenzie, S.R. Miller, T.A. Pugsley, L.D. Wise, Chromeno[3,4-c]pyridin-5-ones: selective human dopamine D 4 receptor antagonists as potential antipsychotic agents, J. Med. Chem. 40 (1997) 2688–2693, https://doi.org/10.1021/jm970170v.

[29] L.V. Frolova, I. Malik, P.Y. Uglinskii, S. Rogelj, A. Kornienko, I.V. Magedov, Multicomponent synthesis of 2,3-dihydrochromeno[4,3-d]pyrazolo[3,4-b]pyridine-1,6-

diones: a novel heterocyclic scaffold with antibacterial activity, Tetrahedron Lett. 52 (2011) 6643–6645, https://doi.org/10.1016/j.tetlet.2011.10.012.

[30] A.D. Bani-Yaseen, M. Al-Balawi, The solvatochromic, spectral, and geometrical properties of nifenazone: a DFT/TD-DFT and experimental study, Phys. Chem. Chem. Phys. 16 (2014) 15519–15526, https://doi.org/10.1039/C4CP01679C.

[31] A.D. Bani-Yaseen, F. Hammad, B.S. Ghanem, E.G. Mohammad, On the photophysicochemical properties of selected fluoroquinolones: solvatochromic and fluorescence spectroscopy study, J. Fluoresc. 23 (2013) 93–101, https://doi.org/10.1007/s10895-012-1120-7.

[32] A. Dawoud Bani-Yaseen, Solvatochromic and fluorescence behavior of sulfisoxazole, J. Fluoresc. ISSN J Fluoresc. 21 (2011)https://doi.org/10.1007/s10895-010-0778-y.

[33] C. Reichardt, Solvatochromic dyes as solvent polarity indicators, Chem. Rev. 94 (1994) 2319–2358, https://doi.org/10.1021/cr00032a005.

[34] D.G. Patel, M.M. Paquette, R.A. Kopelman, W. Kaminsky, M.J. Ferguson, N.L. Frank, A solution- and solid-state investigation of medium effects on charge separation in metastable photomerocyanines, J. Am. Chem. Soc. 132 (2010) 12568–12586, https://doi.org/10.1021/ja100238h.

[35] A. Marini, A. Muñoz-Losa, A. Biancardi, B. Mennucci, What is Solvatochromism? J. Phys. Chem. B 114 (2010) 17128–17135, https://doi.org/10.1021/jp1097487.

[36] A.D. Bani-Yaseen, A.S. Al-Jaber, H.M. Ali, Probing the solute-solvent interaction of an azo-bonded prodrug in neat and binary media: combined experimental and computational study, Sci. Rep. 9 (2019) 3023, https://doi.org/10.1038/s41598-019-39028-1.

[37] A.D. Bani-Yaseen, Computational molecular perspectives on the interaction of propranolol with β-cyclodextrin in solution: towards the drug-receptor mechanism of interaction, J. Mol. Liq. 227 (2017) 280–290, https://doi.org/10.1016/j.molliq.2016.12.023.

[38] A.D. Bani-Yaseen, Computational insights into the photocyclization of diclofenac in solution: effects of halogen and hydrogen bonding, Phys. Chem. Chem. Phys. 18 (2016) 21322–21330, https://doi.org/10.1039/c6cp03671f.

[39] M. Shkoor, H.-L. Su, S. Ahmed, S. Hegazy, Synthesis of 5-oxo-5 H-chromeno[3,4-c] pyridine-1-carbonitriles and features of their NMR spectra, J. Heterocycl. Chem. 57 (2020) 813–819, https://doi.org/10.1002/jhet.3826.

[40] G.E. Frisch, M. J.; Trucks, G. W.; Schlegel, H. B.; Scuseria, V. M. Robb, M. A.; Cheeseman, J. R.; Scalmani, G.; Barone, H. B.; Petersson, G. A.; Nakatsuji, H.; Caricato, M.; Li, X.; Hratchian, M. P.; Izmaylov, A. F.; Bloino, J.; Zheng, G.; Sonnenberg, J. L.; Hada, M. N. Ehara, M.; Toyota, K.; Fukuda, R.; Hasegawa, J.; Ishida, J. T.; Honda, Y.; Kitao, O.; Nakai, H.; Vreven, T.; Montgomery, J. A., E.N. Peralta, J. E.; Ogliaro, F.; Bearpark, M. J.; Heyd, J.; Brothers, J.; Kudin, K. N.; Staroverov, V. N.; Kobayashi, R.; Normand, S.S.; Raghavachari, K.; Rendell, A. P.; Burant, J. C.; Iyengar, J.E.; Tomasi, J.; Cossi, M.; Rega, N.; Millam, N. J.; Klene, M.; Knox, R.. Cross, J. B.; Bakken, V.; Adamo, C.; Jaramillo, J.; Gomperts, C.. Stratmann, R. E.; Yazyev, O.; Austin, A. J.; Cammi, R.; Pomelli, V.G.; Ochterski, J. W.; Martin, R. L.; Morokuma, K.; Zakrzewski, A.; Voth, G. A.; Salvador, P.; Dannenberg, J. J.; Dapprich, S.; Daniels, D.J. D.; Farkas, O.; Foresman, J. B.; Ortiz, J. V.; Cioslowski, J.; A Fox, Gaussian 09, Gaussian, Inc. Wallingford, CT, (n.d.).

[41] J. Tomasi, B. Mennucci, E. Cancès, The IEF version of the PCM solvation method: an overview of a new method addressed to study molecular solutes at the QM ab initio level, J. Mol. Struct. THEOCHEM 464 (1999) 211–226, https://doi.org/10.1016/S0166-1280(98)00553-3.

[42] M.J. Kamlet, J.L.M. Abboud, M.H. Abraham, R.W. Taft, Linear solvation energy relationships. 23. A comprehensive collection of the solvatochromic parameters, .pi.*, . alpha., and .beta., and some methods for simplifying the generalized solvatochromic equation, J. Org. Chem. 48 (1983) 2877–2887, https://doi.org/10.1021/jo00165a018.